Raman Spectroscopy of Dense H₂O and the Transition to Symmetric Hydrogen Bonds

Alexander F. Goncharov, Viktor V. Struzhkin,* Ho-kwang Mao, and Russell J. Hemley

Geophysical Laboratory and Center for High Pressure Research, Carnegie Institution of Washington,
5251 Broad Branch Road, N.W., Washington, D.C. 20015

High-pressure Raman measurements of H_2O ice using synthetic diamond anvils reveal major changes associated with the transition to the nonmolecular, symmetric hydrogen-bonded state. At 60 GPa the strongly pressure-dependent O-H symmetric stretching mode disappears, and the translational modes exhibit frequency and damping anomalies. With further increase in pressure, a single peak appears and becomes the dominant feature in the spectrum in the megabar range. The band is assigned to the predicted Raman-active O-O mode of the nonmolecular phase, consistent with the formation of cuprite-type ice X with static, symmetric hydrogen bonds.

Recent theoretical and experimental studies of ice have uncovered intriguing phenomena in this material at high pressures [1–7]. Of particular interest has been the pressure-induced transformation to nonmolecular forms, a transition connected with hydrogen-bond symmetrization [8–11]. It is becoming increasingly clear that quantum effects play an essential role in governing crucial aspects of the system under pressure (e.g., Refs. [1,2,12]); indeed, the study of ice provides important tests of theoretical treatments of quantum behavior in dense solids in general. Recent infrared (IR) measurements have provided evidence for the transition from ice VII (or ice VIII at lower temperature) to a phase with symmetric hydrogen bonds (ice "X") beginning at 60 GPa and stable to at least 210 GPa [13] (see also Refs. [14,15]). Additional information from x-ray diffraction studies includes an increase in intensity of the hydrogen-related reflection (111) over a wide pressure interval [5] and small changes in the equation of state [6,16].

Major questions now surround the onset and dynamics of the transition, the precise crystal structure (or structures) involved, and the possibility of intermediate phases. First-principles molecular dynamics simulations [2] are in good agreement with the conclusion of the infrared studies but predict the existence of an intermediate regime characterized by large amplitude proton motion prior to the formation of the symmetric state (see also Ref. [10]). Calculations based on approximate single-particle double-well potentials indicate similar behavior, with proton tunneling in the vicinity of the transition which vanishes at higher pressures where the effective potential evolves into a single-well-type [10,13]. It has also been proposed that this change in the underlying effective potential is the actual transition to ice X, and that "disordered" ice X [1,6] or VII [2,10] appears at intermediate pressures.

In principle, Raman spectroscopy is ideal for addressing these issues in dense ice. However, owing to the very low scattering cross section of the material at these pressures, such spectra have been extremely difficult to measure and the results are controversial (see Ref. [17]). The Raman-active stretching mode in H_2O ice softens until it merges into the second-order Raman signal from the diamond anvils at 25 GPa [18]. Lattice translational and rotational modes observed to maximum pressures of 62 and 20 GPa, respectively, have been used to determine the boundary between ice VIII (tetragonal antiferroelectric phase) to ice VII (disordered cubic paraelectric phase) [12,17]. It has been reported, however, that no Raman peaks were observed in measurements carried out at higher pressures (to 130 GPa; see Ref. [6]). Nevertheless, Raman-active vibrations are expected for the high-pressure phase: a single Raman-active T_{2g} phonon is predicted for the predicted Cu_2O-type structure [18], an observation that would be considered a clear diagnostic of the phase. In this Letter, we present Raman spectra of H_2O ice to megabar pressures, which cover the stability fields of ice VII and ice VIII and the transition to higher pressure forms. We find new features in the Raman spectra that can be understood by coupling of the O-H stretch vibration to other modes as the soft mode decreases in frequency with pressure. With a further increase in pressure, a single band emerges that is identified as the expected oxygen vibrational mode of T_{2g} symmetry as predicted for the classical cuprite-type structure of H_2O.

The principal difficulty in high-pressure Raman studies of H_2O has been the presence of background luminescence and Raman scattering from diamond anvils, which is normally much stronger than the weak Raman signal from the sample, and pressure gradients due to the shear strength of ice (e.g., Ref. [16]). We overcame these problems by use of high-purity synthetic diamond anvils [19] in a confocal optical configuration with a tightly focused laser that substantially suppresses the luminescence and spurious Raman signals as well as the effects of pressure gradients on the spectra [20]. Spectra were recorded by a single-grating ISA HR-460 spectrometer equipped with holographic notch filters and a charge-coupled device (CCD) detector. Normally, spectra were collected using

low (300 g/mm grating) and high (1800 g/mm grating) spectral resolution modes. The first mode was used for recording very broad (≤ 1000 cm^{-1}) spectral features, whereas the second (~ 2 cm^{-1} resolution) provided accurate measurement of the narrow bands, including their line shapes. Doubly distilled, deionized water was loaded in modified Mao-Bell diamond-anvil cell. Low-temperature measurements were performed in liquid He continuous flow cryostats with quartz infrasil windows, and the pressure was determined from the ruby R_1 band. Three separate experiments were performed at 3–128 GPa and 10–300 K. We systematically measured spectra along the isotherms at 295 and 20–30 K, and along several quasi-isobars; we also made numerous traverses of the VII-VIII transition line. We also crossed the 60–80 GPa region several times by increasing and decreasing pressure under isothermal conditions.

Representative Raman spectra are shown in Fig. 1. The high-frequency O-H stretching vibrations in H_2O ice VIII form a triplet (a doublet and a small shoulder), which has been assigned to $\nu_1(A_{1g})$, $\nu_3(E_g)$, and $\nu_1(B_{1g})$ modes in order of increasing frequency (ice VIII, point group D_{4h}) [18]. As in Refs. [7,17,18], we observe softening of these modes with pressure. Despite the merging with the second-order band from the diamond anvils at 22 GPa, we were able to track the behavior of these bands by subtracting the signal from the diamond taken as a reference at 17 GPa. The high-frequency $\nu_1(A_{1g})$ band has the largest pressure shift. We find that as this mode decreases in frequency, the intensities of the other bands (descriptions given below) are enhanced sequentially from higher to lower frequency to produce prominent resonances which
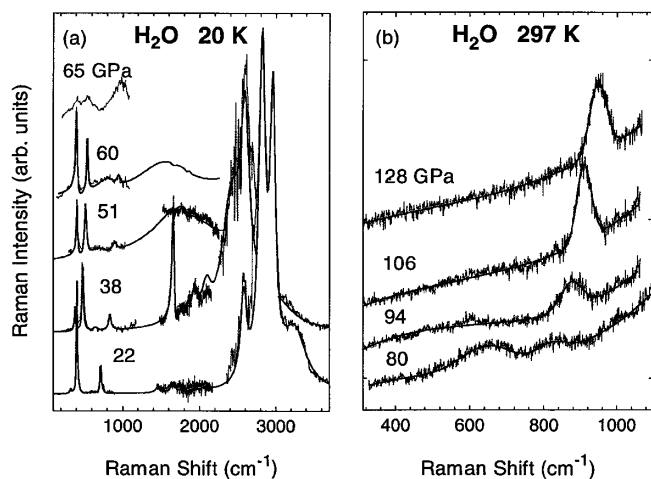

FIG. 1. (a) Representative Raman spectra at 22–65 GPa and 20 K. The points are the experimental data. First- and second-order Raman signal from diamond anvils is subtracted. The lines represent the results of the coupled oscillator model (see text for details). The data in the 1700–2200 cm^{-1} range were measured with higher resolution and hence have a lower signal-to-noise ratio. (b) Raman spectra (uncorrected) at 70–128 GPa and room temperature. The line is a phenomenological fit.
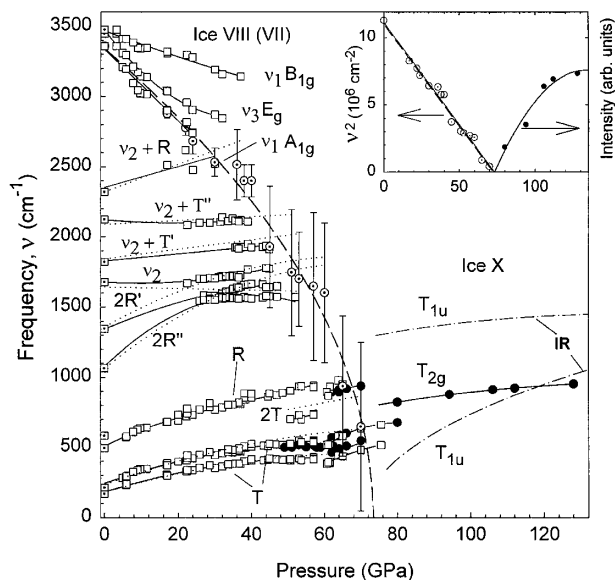
appear and disappear as the pressure increases. Most notable, for example, is the enhancement of the 1650 cm^{-1} band at 38 GPa and the 400 cm^{-1} band at 51 and 60 GPa (Fig. 1a).

Measurements in the low-frequency range reveal several important changes. We find a change in the spectrum at 55–62 GPa at all temperatures. Sharp translational bands at 400 and 500 cm^{-1} assigned to the $\nu_{T_z}(A_{1g}) + \nu_{T_{xy}}(E_g)$ and $\nu_{T_z}(B_{1g}) + \nu_{T_{xy}}(E_g)$ excitations, respectively, of ice VIII exhibit only minor frequency shifts at 45–60 GPa; they soften and broaden just above 60 GPa and then increase in frequency with pressure. Changes are also observed near 60 GPa in a broad band at 700 cm^{-1}, which appears only at high pressure. At $T > 100$ K the broad translational band of ice VII at 500 cm^{-1}, which correlates with the $\nu_{T_z}(B_{1g}) + \nu_{T_{xy}}(E_g)$ band of ice VIII, evolves into a doublet. These changes near 60 GPa become less pronounced as temperature increases: the linewidth of the lowest frequency band of the doublet increases with temperature, and both lower bands tend to increase in frequency (Fig. 2) and become an unresolved doublet at room temperature. The intensity of the rotational band gradually decreases and disappears in approximately the same pressure range. In contrast to these relatively minor changes, further increase in pressure produces a major alteration in the Raman spectrum. At 80–90 GPa, a new narrow band appears (Fig. 1b), while the other excitations appear to weaken. The frequency of this new excitation increases with pressure, with little qualitative change in the spectrum between 100 and 128 GPa (the small increase in linewidth of the 900 cm^{-1} mode can be explained by increasing pressure gradients). Numerous control experiments have established that the peak is associated with the sample and not stress-induced changes in the diamond Raman [21]. The peak is the dominant Raman band in H_2O at these pressures.

To interpret these spectra, we applied a multiple coupled oscillator model to the observed Raman modes. Following a well-known formalism (e.g., Ref. [22]), we determined the spectra from the imaginary part of the complex susceptibility for the coupled modes in terms of the corresponding Green's function and mode strengths. The inverse of the frequency-dependent Green's function of a single oscillator is $G_{ii}^{-1}(\omega) = \Omega_i^2 - \omega^2 - i\omega\gamma_i$ (where Ω_i is the ith oscillator frequency and γ_i is its damping constant); the inverse Green's function of the system of coupled oscillators is given by

$$G^{-1}(\omega) = \|G_{ii}^{-1}(\omega)\| + \|V_{ij}^2\|, \qquad (1)$$

where $\|G_{ii}^{-1}\|$ is a matrix having single oscillator inverse Green's functions on the diagonal (nondiagonal elements equal to zero), and $\|V_{ij}^2\|$ is a nondiagonal matrix with coupling strengths between oscillators i and j (diagonal elements equal to zero). The response of the system of such coupled oscillators in terms of $G(\omega)$ from Eq. (1) is

FIG. 2.   Raman frequencies of H_2O to 128 GPa. Changes in intensities and pressure dependences of the lower frequency modes are observed at 60 and ~80 GPa, as described in the text. The open squares are measured frequencies at 20 K; black circles correspond to room temperature. The observed frequency shifts are indicated by the solid lines (guides to the eye). The low-pressure data (<30 GPa) agree with previous measurements (e.g., Refs. [7,18]). The ambient pressure data (dotted open squares) are from Ref. [23]; the high-pressure IR data (dotted-dashed lines) are from Ref. [13]. The dotted lines are the bare frequencies obtained from the coupled oscillator model for ice VIII: $\Omega_{T1} = 176.8 + 8.06P - 0.06P^2$; $\Omega_{T2} = 235.7 + 9.13P - 0.05P^2$; $\Omega_{2T} = 529.6 + 4.8P$; $\Omega_{2R''} = 1061.9 + 21.3P - 0.15P^2$; $\Omega_{2R'} = 1360.9 + 14.4P - 0.10P^2$; $\Omega_2 = 1642 - 0.55P$; $\Omega_{2+T'} = 1843 + 3.35P$; $\Omega_{2+T''} = 2090 + 1.33P$; $\Omega_{2+R} = 2330 + 9.8P$; the coupling parameters are $V_{SM-\nu_{T1}} = 500$; $V_{SM-\nu_{T2}} = 600$; $V_{SM-\nu_{2T}} = 600$; $V_{SM-\nu_{2R''}} = 580$; $V_{SM-\nu_{2R'}} = 480$; $V_{SM-\nu_2} = 400$; $V_{SM-\nu_2+T'} = 425$; $V_{SM-\nu_2+T''} = 550$; $V_{SM-\nu_2+R} = 650$, where the pressure is in GPa, frequency is in cm^{-1}, and SM denotes the soft mode. The soft mode bare frequency (dotted circles) is shown with the associated errors; the dashed line indicates the fitted pressure dependence. In general, a parabolic dependence of V_{ij} on pressure improves the fit, additional details of the model will be presented elsewhere [28]. For mode definitions see Refs. [15,18] (the assignment of combination bands is tentative). Inset: pressure dependence of the square of the soft mode frequency and intensity of the single peak in the high-pressure phase (points and solid line). The dashed line is the extrapolation of the soft mode given in Ref. [7] based on lower pressure measurements.

given by

$$I(\omega) = \text{Im}\left(\sum_{ij} \omega_p^i G_{ij}(\omega) \omega_p^j \right), \qquad (2)$$

where ω_p^i denotes the plasma frequency (strength) of the ith oscillator.

We simulated the observed spectra by a superposition of the soft mode and a number of oscillators that are either coupled or uncoupled to it. These bands include defor-

mational (ν_2), translational and rotational modes, and their combinations [15,23]. Fits of the frequency shifts of the modes at lower pressures were used to probe the coupling with the soft mode at higher pressures. The parameters of the model were determined by fitting the simulated to the measured spectra. This procedure gave the pressure dependence of mode parameters (frequencies, strengths, linewidths, and couplings; e.g., Fig. 2). Very good agreement with experiment is obtained (Fig. 1a). Both the observed intensity increases (e.g., large enhancement of ν_2 near 1650 cm^{-1}) and asymmetries of the peaks can be explained by the coupling of the modes to the soft mode [24].

The soft mode itself is not observable above 40 GPa, but we have been able to constrain its frequency, linewidth, and strength (Fig. 2) by analyzing its coupling with other observable modes. To reproduce the spectra at these pressures the strength of the soft mode must decrease. Of special interest is the coupling of the soft mode to the two low-frequency translational modes and the 700 cm^{-1} mode at about 60 GPa. This behavior can be understood by assuming a crossover of these modes with the overdamped soft mode. If we assume that near the transition $\Omega_{SM} = A(P_c - P)^\alpha$ ($\alpha = 1/2$ is the critical index, P_c is the critical pressure), as suggested by low-pressure Raman measurements [7], then we can obtain very good fits over the entire pressure range. This analysis is in excellent agreement with the direct observations of the spectrum of the high-pressure phase. But the most significant result of this study is the direct observation of the single phonon excitation which grows in intensity between 80 and 95 GPa and persists to the maximum pressure (128 GPa). A fit of the intensity versus pressure gives an onset pressure (P_c) near 70 GPa (Fig. 2 inset). The new band is identified as the T_{2g} (first-order) O-O vibration as expected for the Cu_2O structure, which is consistent with available x-ray data [26]. Combined with the two IR-active T_{1u} modes (Fig. 2), this completes the identification of the $\mathbf{k} = 0$ vibrational spectrum of ice X.

The phase diagram determined from these measurements is shown in Fig. 3. The VII-VIII boundary, determined from changes in the low-frequency modes, is in good agreement with the Raman studies reported in Refs. [7,17]. The pressure at which the T_{2g} mode appears is comparable to that estimated from the extrapolation of the high-frequency O-H Raman mode from low pressure, providing further support for the soft-mode character of the transition. Comparison of the low-temperature Raman data for the ice VII-VIII line (where the sharp low-frequency bands disappear) with the room- [15] and liquid-nitrogen- [13] temperature IR studies (as well as with the pressure of the possible compressibility changes from x-ray measurements [6]) suggests a possible triple point. However, the changes in the Raman spectra measured as a function of temperature near 60 GPa (Fig. 3) can also occur as a result of mode coupling, so the existence
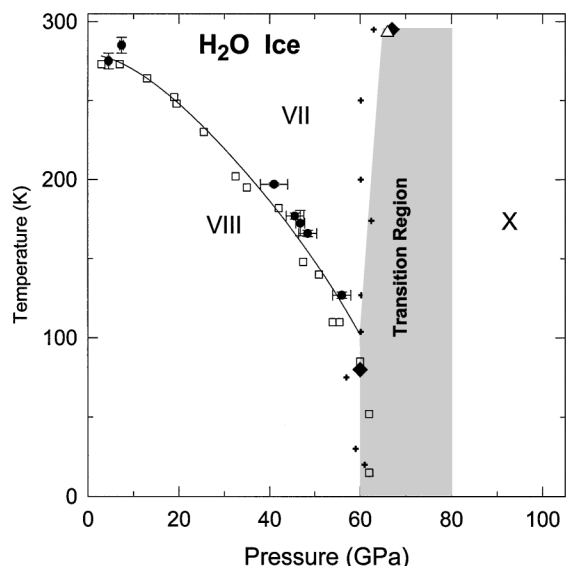
FIG. 3. Phase diagram of H_2O. Solid circles, this work; open squares [17]; closed diamond, IR [13,15]; open triangle, x ray [6,16]. The crosses denote the points where changes in the low-frequency modes are observed, and the grey area indicates the transition region between the low- and high-pressure phases (see text).

of a well-defined (vertical) phase line at this pressure remains to be established; understanding this transition region above 60 GPa thus requires further study. With increase in pressure within the high-pressure phase, quantum proton motion becomes suppressed as a result of the reduction of the barrier in the original double-well effective potential, giving rise to a single well-type potential. At this point (e.g., >100 GPa), the Raman spectra obey momentum conservation rules and symmetry restrictions to produce one first-order excitation in the classical high-pressure structure [9,13,27].

*Permanent address: Inst. for High Pressure Phys., Russ. Acad. of Sci., 142092 Troitsk, Moscow Region, Russia.

[1] M. Benoit, D. Marx, and M. Parrinello, Nature (London) **392**, 258 (1998).

[2] M. Bernasconi, P. L. Silvestrelli, and M. Parrinello, Phys. Rev. Lett. **81**, 1235 (1998).

[3] J. S. Tse and D. D. Klug, Phys. Rev. Lett. **81**, 2466 (1998).

[4] R. J. Nelmes et al., Phys. Rev. Lett. **81**, 2719 (1998).

[5] P. Loubeyre, R. LeToullec, E. Wolanin, M. Hanfland, and D. Häusermann, Nature (London) **397**, 503 (1999).

[6] E. Wolanin et al., Phys. Rev. B **56**, 5781 (1997).

[7] Ph. Pruzan et al., J. Phys. Chem. B **101**, 6230 (1997).

[8] B. Kamb and B. Davis [Proc. Natl. Acad. Sci. U.S.A. **52**, 1433 (1964)] presented an early discussion of the possibility of symmetric hydrogen bonds formed from compression of ice VII.

[9] W. B. Holzapfel, J. Chem. Phys. **56**, 712 (1972).

[10] F. H. Stillinger and K. S. Schweizer, J. Phys. Chem. **87**, 4281 (1983); K. S. Schweizer and F. H. Stillinger, J. Chem. Phys. **80**, 1230 (1984).

[11] C. Lee, D. Vanderbilt, K. Laasonen, R. Car, and M. Parrinello, Phys. Rev. Lett. **69**, 462 (1992).

[12] Ph. Pruzan, J. C. Chervin, and B. Canny, J. Chem. Phys. **99**, 9842 (1993).

[13] A. F. Goncharov, V. V. Struzhkin, M. S. Somayazulu, R. J. Hemley, and H. K. Mao, Science **272**, 149 (1996).

[14] K. Aoki, H. Yamawaki, M. Sakashita, and H. Fujihisa, Phys. Rev. B **54**, 15 673 (1996).

[15] V. V. Struzhkin, A. F. Goncharov, R. J. Hemley, and H. K. Mao, Phys. Rev. Lett. **78**, 4446 (1997).

[16] R. J. Hemley et al., Nature (London) **330**, 737 (1987); R. J. Hemley and H. K. Mao, *Properties of Earth and Planetary Materials at High Pressures and Temperatures,* edited by M. H. Manghnani and T. Yagi (A.G.U., Washington, D.C., 1998), p. 173.

[17] Ph. Pruzan, J. C. Chervin, and B. Canny, J. Chem. Phys. **97**, 718 (1992).

[18] K. R. Hirsch and W. B. Holzapfel, J. Chem. Phys. **84**, 2771 (1986).

[19] The diamonds were chemically pure crystals obtained from General Electric Superabrasives, Worthington, Ohio.

[20] The system uses spatial filtering with the depth of focus reduced by focusing the exciting laser radiation (476.5, 488, and 514.5 nm argon-ion lines) down to 2 μm in a backscattering geometry using the entire aperture of the microscope objective.

[21] P. G. Johannsen, J. Phys. Condens. Matter **10**, 1 (1998).

[22] R. S. Katiyar, J. F. Ryan, and J. F. Scott, Phys. Rev. B **4**, 2635 (1971).

[23] P. T. T. Wong and E. Whalley, J. Chem. Phys. **64**, 2359 (1976).

[24] The intensity ratio R for a pair of coupled modes can be described semiquantitatively by $R = (\Delta\omega - \Delta\Omega)/(\Delta\omega + \Delta\Omega)$, where $\Delta\Omega$ is the difference in bare frequencies, and $(\Delta\omega)^2 = (\Delta\Omega)^2 + V^2$ is the squared difference in observed mode frequencies (e.g., Ref. [25]). Pressure-dependent changes in parameters of the model (see Fig. 2 caption) can give rise to a stonger resonance increase in intensity (as observed for the 1650 cm^{-1} band) than is predicted by this formula.

[25] K. Aoki, H. Yamawaki, and M. Sakashita, Science **268**, 1322 (1995).

[26] Other structures that would be consistent with the spectrum include those based on an hcp oxygen framework, which would give rise to a Raman-active oxygen translational mode; however, this structure is inconsistent with the reported x-ray data (e.g., Refs. [5,6,16]).

[27] W. B. Holzapfel, Physica (Amsterdam) **265B**, 113 (1999).

[28] V. V. Struzhkin et al. (to be published).